

Research Article

DOA Estimation for Non-Gaussian Signals: Three-Level Nested Array and a Successive SS-MUSIC Algorithm

Sha Shi ^{1,2}, Haowei Zeng ^{1,2}, Heng Yue ^{1,2}, Changbo Ye ^{1,2} and Jianfeng Li ^{1,2}

¹College of Electronic Information Engineering, Nanjing University of Aeronautics and Astronautics, Nanjing, China

²Key Laboratory of Dynamic Cognitive System of Electromagnetic Spectrum Space,

Nanjing University of Aeronautics and Astronautics, Ministry of Industry and Information Technology, Nanjing 211106, China

Correspondence should be addressed to Sha Shi; shisha@nuaa.edu.cn

Received 14 December 2021; Revised 28 February 2022; Accepted 11 March 2022; Published 7 April 2022

Academic Editor: Xianpeng Wang

Copyright © 2022 Sha Shi et al. This is an open access article distributed under the Creative Commons Attribution License, which permits unrestricted use, distribution, and reproduction in any medium, provided the original work is properly cited.

Direction of arrival (DOA) estimation for non-Gaussian signals using three-level nested array (THL-NA) is investigated in this paper. Motivation from larger consecutive degree of freedom (DOF) and array aperture, the THL-NA is proposed, which can take full advantages of the consecutive coarrays of TL-NA and has the closed-form expression of DOF. Specifically, firstly, the array aperture is expanded by the second order sum coarray (2-SC) of the proposed array, secondly, the nested relationship between subarrays is employed to obtain the difference coarray of 2-SC (2-DCSC), finally, a consecutive virtual array with large array aperture is obtained. Besides, a successive SS-MUSIC algorithm is proposed, which employs the spatial smoothing estimating signal parameter via rotational invariance techniques (SS-ESPRIT) algorithm and partial spectrum searching multiple signal classification (PSS-MUSIC) to obtain initial estimations and fine estimations, respectively, resulting in a better balance between computational complexity and estimation accuracy.

1. Introduction

Direction of arrival (DOA) estimation, which is one of the fundamental issues in array signal processing, plays an important role in various fields, e.g., radar systems, acoustics, navigation, and wireless communications [1–3].

Compared with traditional uniform linear arrays (ULAs), sparse arrays can obtain less mutual coupling and higher degrees of freedom (DOF), which can obtain DOA estimation for signals with more sources. The nested array (NA) [4] is a sparse array composed of two ULAs with different spacings, which has strong expansion capability in DOA estimation algorithms based on FOC. The coprime array (CPA) [5, 6], consisting of two ULAs with coprime interelement spacings, has less mutual coupling compared with NA. These arrays can generate sets of uniformly distributed virtual second order difference coarray (2-DC) [4], in particular, the 2-DC of NA is free from holes. However, these sparse arrays have limitations due to their array geometries. The 2-DC of CPA generates a lot of holes that

decrease consecutive DOF significantly, the dense part of NA leads to more serious mutual coupling than CPA.

Traditional DOA parameter estimation algorithms, such as multiple signal classification (MUSIC) algorithm [7, 8] and estimation of signal parameters via rotational invariance techniques (ESPRIT) algorithm [9, 10], mostly utilize the second order statistical characteristics of the signals. Furthermore, new algorithms have been proposed such as 2D-MUSIC and RD-MUSIC [1]. When the signals obey the Gaussian distribution, they can be described by the first order or second order statistics. However, the situation in practical applications is more complicated, and most sources to be processed are non-Gaussian signals, whose statistical characteristics can be described by fourth order cumulant (FOC) [11, 12], resulting in larger array aperture and better DOA estimation performance, as compared with second order cumulant (SOC). Considering the non-Gaussian signals, DOA estimation methods based on FOC, including MUSIC-LIKE [13, 14] and virtual-ESPRIT algorithm [15], are most exploited. The virtual coarrays utilized by

vectorized FOC methods can be obtained from fourth order difference coarray (4-DC) [16] or difference coarray of sum coarray (2-DCSC) [17] operation of physical sensors. The FOC can not only suppress Gaussian white noise or color noise, but effectively expand the length of array apertures. Therefore, the estimation performance of DOA based on FOC is greatly improved.

Combining the designing of sparse array and the exploiting of 4-DC or 2-DCSC, lots of array structures are proposed, such as fourth-level NA (FL-NA) [16], sparse array with fourth order difference coarray enhancement based on CPA (SAFE-CPA) [18]. FL-NA is investigated in detail as a special case of $2q$ -level NAs when q is equal 2 in reference [16] and SAFE-CPA constructs physical sensors structure by adding another subarray. Regarding the processing of the above sparse array structure, related scholars have proposed a series of FOC estimation algorithms based on spatial smoothing subspace methods [19, 20] such as SS-MUSIC algorithm, SS-ESPRIT algorithm, which provide a theoretical basis for the DOA estimation based on sparse arrays.

In this paper, a novel sparse array structure, named three-level nested array (THL-NA), is proposed for non-Gaussian incident signals, which can take full advantages of the consecutive coarrays of TL-NA and has the closed-form expression of DOF. Firstly, the 2-SC [21] of the proposed array is obtained to expand the array aperture, and then the consecutive 2-DCSC of the proposed array is obtained by employing the nested relationship between subarrays of 2-SC. To make a better balance between computational complexity and estimation accuracy, a successive SS-MUSIC algorithm is proposed, which employs the spatial smoothing ESPRIT (SS-ESPRIT) algorithm and partial spectrum searching MUSIC (PSS-MUSIC) to obtain initial estimates and fine estimates, respectively.

The three contributions of this paper are extracted as follows:

- (1) From the viewpoint of constructing sum or difference coarray, the THL-NA based on the FOC is proposed to obtain large consecutive DOF and array aperture, which enhances the DOA estimation performance.
- (2) From the perspective for expressing the length of the virtual array in the THL-NA, this paper derives the closed-form expressions with consecutive DOF and discusses the optimal array configuration to achieve the largest consecutive DOF.
- (3) In terms of making a balance between computational complexity and estimation accuracy, a successive SS-MUSIC algorithm is proposed, which employs SS-ESPRIT algorithm and PSS-MUSIC to obtain initial angle estimations and fine angle estimations, respectively.

The chapter arrangement of this paper is as follows. In Section 2, we introduce 2-DC, 2-SC, 2-DCSC, 4-DC, and the properties of NA. We elaborate the array configuration of THL-NA and explain the closed-form expression in Section

3. The proposed algorithm called successive SS-MUSIC algorithm is presented in Section 4. Section 5 analyzes the performance of THL-NA and the computational complexity of the successive SS-MUSIC algorithm. Section 6 provides lots of simulations and the conclusions are drawn in Section 7.

Notations. Throughout the paper, matrices are expressed by upper-case bold characters and vectors are denoted by lower-case bold characters, respectively. $(\cdot)^T$, $(\cdot)^H$, $(\cdot)^{-1}$, and $(\cdot)^*$ imply the transpose, the conjugate transpose operation, inverse and complex conjugation of a vector or matrix, respectively. \otimes , \odot , and \oplus stand for the Kronecker product, Khatri-Rao product and Hadamard product, respectively. $\text{vec}(\cdot)$ represents the vectorization operation and $\text{cum}(\cdot)$ indicates the cumulant operator. $\text{angle}(\cdot)$ signifies the phase operator and $\|\cdot\|_F$ shows the Frobenius norm. $\arcsin(\cdot)$ means the arcsine function.

2. Preliminaries

In this section, the 2-DC, 2-SC, 2-DCSC, 4-DC, and the properties of NA are introduced.

2.1. The Definitions of 2-DC, 2-SC, 4-DC, and 2-DCSC. Consider a P -sensors linear array, whose locations set can be indicated as [22]

$$S = \{v_1 \cdot d, v_2 \cdot d, \dots, v_P \cdot d\}, \quad (1)$$

where $v_p \cdot d$ represents the position of the p -th sensor, $p = 1, 2, \dots, P$, and d is the unit spacing.

Definition 1. For the array with the set of sensor position S in equation (1), the 2-DC set is defined as [17]

$$C_{2\text{-DC}} = \Phi_{2\text{-DC}} d, \quad (2)$$

where the set of 2-DC lags

$$\Phi_{2\text{-DC}} = \{v_{p1} - v_{p2}, 1 \leq p1, p2 \leq P\}. \quad (3)$$

Definition 2. The 2-SC set is defined as [21]

$$C_{2\text{-SC}} = \Phi_{2\text{-SC}} d, \quad (4)$$

with the set of 2-SC lags

$$\Phi_{2\text{-SC}} = \{v_{p1} + v_{p2}, 1 \leq p1, p2 \leq P\}. \quad (5)$$

Definition 3. The 4-DC set is defined as [16]

$$C_{4\text{-DC}} = \Phi_{4\text{-DC}} d, \quad (6)$$

where the set of 4-DC lags

$$\Phi_{4\text{-DC}} = \{(v_{p1} - v_{p2}) - (v_{p3} - v_{p4}), 1 \leq p1, p2, p3, p4 \leq P\}. \quad (7)$$

Definition 4. The 2-DCSC set is defined as [17]

$$C_{2\text{-DCSC}} = \Phi_{2\text{-DCSC}} d, \quad (8)$$

where the set of 2-DCSC lags

$$\Phi_{2\text{-DCSC}} = \{(v_{p1} + v_{p2}) - (v_{p3} + v_{p4}), \quad 1 \leq p1, p2, p3, p4 \leq P\}. \quad (9)$$

By permutation invariance, $\Phi_{2\text{-DCSC}}$ can be rewritten as

$$\Phi_{2\text{-DCSC}} = \{(v_{p1} - v_{p2}) - (v_{p3} - v_{p4})\} = \{(v_{p1} + v_{p4}) - (v_{p2} + v_{p3})\} = \Phi_{4\text{-DC}}. \quad (10)$$

for $1 \leq p1, p2, p3, p4 \leq P$. That is, for a particular array, the 4-DC is equivalent to the 2-DCSC

$$C_{4\text{-DC}} = C_{2\text{-DCSC}}. \quad (11)$$

2.2. The Properties of TL-NA. The configuration of TL-NA [4] has been shown in Figure 1, which contains two sparse uniform subarrays. The first subarray has M_1 sensors with interelement spacing d , where $d = \lambda/2$ and λ is the

wavelength, while the another subarray has M_2 sensors with interelement spacing $(M_1 + 1)d$. The position of TL-NA varies from $1d$ to $M_2(M_1 + 1)d$ and it can be represented as

$$S = \{m_1 d, 1 \leq m_1 \leq M_1\} \cup \{m_2 (M_1 + 1)d, 1 \leq m_2 \leq M_2\}. \quad (12)$$

Refer to Definition 1, the 2-DC location set of TL-NA can be written as

$$C_{2\text{-DC}} = \{-M_2(M_1 + 1) + 1, \dots, -1, 0, 1, \dots, M_2(M_1 + 1) - 1\}d. \quad (13)$$

Refer to Definitions 3 and 4, the 4-DC (2-DCSC) location set of TL-NA can be expressed as [23]

$$C_{4\text{-DC}} = C_{2\text{-DCSC}} = \{-2M_2(M_1 + 1) + 2, \dots, -1, 0, 1, \dots, 2M_2(M_1 + 1) - 2\}d. \quad (14)$$

From equations (13) and (14), It can be concluded that the position of the 2-DC and 2-DCSC of TL-NA are consecutive.

2.3. Data Model Based on FOC. Assume K far-field narrowband uncorrelated sources impinging upon the array with locations set S from directions $\theta = [\theta_1, \dots, \theta_K]$, the

received data model of the array can be expressed as [24, 25]

$$\mathbf{x}(t) = \mathbf{A}\mathbf{s}(t) + \mathbf{n}(t), \quad (15)$$

where $\mathbf{A}(\theta) = [\mathbf{a}(\theta_1), \mathbf{a}(\theta_2), \dots, \mathbf{a}(\theta_K)] \in \mathbb{C}^{P \times K}$ represents the steering matrix of array, and the steering vector at direction θ_k , which denotes the elevation angle of the k -th target, is given by

$$\mathbf{a}(\theta_k) = [e^{-j2\pi v_1 d \sin \theta_k / \lambda}, e^{-j2\pi v_2 d \sin \theta_k / \lambda}, \dots, e^{-j2\pi v_P d \sin \theta_k / \lambda}]^T \in \mathbb{C}^{P \times 1}. \quad (16)$$

and $\mathbf{s}(t) = [\mathbf{s}_1(t), \mathbf{s}_2(t), \dots, \mathbf{s}_K(t)]^T \in \mathbb{C}^{K \times 1}$, $1 \leq t \leq L$ denotes non-Gaussian signal source matrix with zero mean, where L indicates the number of snapshots. And, $\mathbf{n}(t)$ is the

received additive white Gaussian noise with mean zero and variance σ^2 .

In this paper, for given $x_{k1}, x_{k2}, x_{k3}^*, x_{k4}^*$, the FOC definition can be written as [26]



FIGURE 1: Two-level nested array.

$$\begin{aligned} \mathbf{C}_4 &= \text{Cum}(x_{k_1}, x_{k_2}, x_{k_3}^*, x_{k_4}^*) \\ &= E(x_{k_1} x_{k_2} x_{k_3}^* x_{k_4}^*) - E(x_{k_1} x_{k_2})E(x_{k_3}^* x_{k_4}^*) - E(x_{k_1} x_{k_3}^*)E(x_{k_2} x_{k_4}^*) - E(x_{k_1} x_{k_4}^*)E(x_{k_2} x_{k_3}^*). \end{aligned} \quad (17)$$

For the array, the FOC of the received signal can be [26]

$$\begin{aligned} \mathbf{C}_{4,X} &= \text{Cum}(\mathbf{X}, \mathbf{X}, \mathbf{X}^*, \mathbf{X}^*) \\ &= E[(\mathbf{X} \otimes \mathbf{X}^*)(\mathbf{X} \otimes \mathbf{X}^*)^H] - E(\mathbf{X} \otimes \mathbf{X}^*)E[(\mathbf{X} \otimes \mathbf{X}^*)^H] - E(\mathbf{X}\mathbf{X}^H) \otimes E[(\mathbf{X}\mathbf{X}^H)^*]. \end{aligned} \quad (18)$$

The FOC matrix of the received signal is expressed by [26]

$$\mathbf{R}_4 = \mathbf{C}_{4,X} \quad (19)$$

where

$$\begin{aligned} \mathbf{B}(\theta) &= [\mathbf{b}(\theta_1), \mathbf{b}(\theta_2), \dots, \mathbf{b}(\theta_K)] \\ &= [\mathbf{a}(\theta_1) \otimes \mathbf{a}^*(\theta_1), \mathbf{a}(\theta_2) \otimes \mathbf{a}^*(\theta_2), \dots, \mathbf{a}(\theta_K) \otimes \mathbf{a}^*(\theta_K)] \\ &= \mathbf{A}(\theta) \otimes \mathbf{A}^*(\theta), \\ \mathbf{C}_S &= E[(\mathbf{S} \otimes \mathbf{S})(\mathbf{S} \otimes \mathbf{S})^H] - E(\mathbf{S} \otimes \mathbf{S})E[(\mathbf{S} \otimes \mathbf{S})^H] - E(\mathbf{S}\mathbf{S}^H) \otimes E[(\mathbf{S}\mathbf{S}^H)^*]. \end{aligned} \quad (20)$$

$\mathbf{B}(\theta)$ is the steering matrix after array manifold ($\mathbf{A}(\theta) \Rightarrow \mathbf{B}(\theta)$) by using the FOC. To further improve the performance of DOA estimation, we use a vectorized method [23, 26, 27] for \mathbf{R}_4 to obtain a vector, which is equivalent to the received signal from the virtual ULA.

$$\mathbf{z} = \text{vec}(\mathbf{R}_4) \quad (21)$$

where

$$\begin{aligned} \Lambda(\theta) &= [\mathbf{b}^*(\theta_1) \otimes \mathbf{b}(\theta_1), \mathbf{b}^*(\theta_2) \otimes \mathbf{b}(\theta_2), \dots, \mathbf{b}^*(\theta_K) \otimes \mathbf{b}(\theta_K)] \\ &= \mathbf{B}^*(\theta) \otimes \mathbf{B}(\theta), \end{aligned} \quad (22)$$

and $\mathbf{p} = [c_{4,s_1}, c_{4,s_2}, \dots, c_{4,s_K}]^T$ represents the FOC matrix of source vector, and c_{4,s_k} represents the FOC of the k -th source vector.

2.4. Data Model with Mutual Coupling Based on FOC. Equation (16) assumes that the sensors in the array has not interference with each other. Actually, the output of each sensor is influenced by its adjacent elements owing to the presence of mutual coupling. Therefore, by introducing a mutual coupling matrix \mathbf{C} , the received data model can be rewritten as follows [28, 29].

$$\mathbf{x}(t) = \mathbf{C}\mathbf{A}\mathbf{s}(t) + \mathbf{n}(t), \quad (23)$$

where the mutual coupling \mathbf{C} can be obtained from reference [28], whose define is determined by varieties of factors involving in the distance between sensors, the operating frequency, e.g., and it can be approximated by employing the B-banded model [30–32].

$$\mathbf{C}_{i,j} = \begin{cases} 0, & |v_i d - v_j d| > B, \\ c_{|v_i d - v_j d|}, & |v_i d - v_j d| \leq B, \end{cases} \quad (24)$$

where $v_i d, v_j d \in S$ and $1 = c_0 > |c_1| > \dots > |c_B| > |c_{B+1}| = 0$, $c_1 = 0.3e^{j\pi/3}$, $c_l = c_1 e^{-j(l-1)\pi/8}/l$, for $l \in [2, B]$, $B = 100$ represents the maximum spacing of sensor pairs with mutual coupling. Besides, for a given array, the total strength of the

mutual coupling effect can be measured by coupling leakage as [22, 28]

$$L(\mathbf{M}) = \frac{\|\mathbf{C} - \text{diag}\{\mathbf{C}\}\|_F}{\|\mathbf{C}\|_F}, \quad (25)$$

Based on the mutual coupling model in equation (24), the received signal from the virtual array in equation (21) can be reconstructed as

$$\tilde{\mathbf{z}} = \mathbf{C}_{\text{vec}} \mathbf{\Lambda}(\theta) \mathbf{p}, \quad (26)$$

where $\mathbf{C}_{\text{vec}} = (\mathbf{C} \otimes \mathbf{C}^*)^* \otimes (\mathbf{C} \otimes \mathbf{C}^*)$.

3. The Proposed Array

In this section, the proposed array is specifically introduced, including the position of physical sensors, the derivation of the consecutive elements part in the 2-SC and the 2-DCSC, and the properties of it. Next, we analyze the 2-SC and the 2-DCSC of the array for given parameters, and reveal the influence of different array configurations on the consecutive DOF of the array with the same total number of physical sensors.

3.1. Array Structure. Motivation from larger consecutive DOF and array aperture, the THL-NA is proposed, which has a concrete closed expression form with consecutive DOF. The 2-SC of the proposed array is employed to enlarge the array aperture, and then a consecutive virtual array with large array aperture is obtained by performing the difference operation on the 2-SC, whose consecutive character utilizes the nested relationship between subarrays in the 2-SC. Next, the position of physical sensors in the proposed array is given.

Proposition 1. *The THL-NA is composed of three ULAs with a dense ULA and two sparse ULAs, which is shown in*

$$\begin{aligned} S_1 &= \{n_1 d, 2 \leq n_1 \leq (N_1 + 1)(N_2 + 1)\}, \\ S_2 &= (N_1 + 1)(N_2 + 1)d + \{n_1 d, 1 \leq n_1 \leq N_1\} \cup \{n_2(N_1 + 1)d, 1 \leq n_2 \leq N_2 + 1\}, \\ S_3 &= 2(N_1 + 1)(N_2 + 1)d + \{n_1 d, 1 \leq n_1 \leq N_1\} \cup \{n_2(N_1 + 1)d, 1 \leq n_2 \leq N_2 + 1\}, \\ &\vdots \\ S_{N_3+1} &= N_3(N_1 + 1)(N_2 + 1)d + \{n_1 d, 1 \leq n_1 \leq N_1\} \cup \{n_2(N_1 + 1)d, 1 \leq n_2 \leq N_2\} \cup \{n_3(N_2 + 1)(N_1 + 1)d, 1 \leq n_3 \leq N_3\}, \\ S_{2\text{-SC}} &= S_1 \cup S_2 \cup \dots \cup S_{N_3+1}. \end{aligned} \quad (28)$$

According to the consecutive character of the 2-DC of the TL-NA, it can be seen that a virtual consecutive 2-DCSC is obtained by performing another difference operation on the 2-SC.

Figure 2. The position of THL-NA sensors can be represented as

$$\begin{aligned} S_1 &= \{n_1 d, 1 \leq n_1 \leq N_1\}, \\ S_2 &= \{n_2(N_1 + 1)d, 1 \leq n_2 \leq N_2\}, \\ S_3 &= \{n_3(N_2 + 1)(N_1 + 1)d, 1 \leq n_3 \leq N_3\}, \\ S_{\text{THL-NA}} &= S_1 \cup S_2 \cup S_3. \end{aligned} \quad (27)$$

Figure 2 shows the distribution position of physical sensors in the proposed array. The array consists of three ULAs. The number of sensors is N_1 with interelement spacing d starting from $1d$ in the first subarray, the number of sensors is N_2 with interelement spacing $(N_1 + 1)d$ starting from $(N_1 + 1)d$ in the second subarray and the number of sensors is N_3 with interelement spacing $(N_2 + 1)(N_1 + 1)d$ starting from $(N_2 + 1)(N_1 + 1)d$ in the third subarray. The total number of physical sensors is N and $N = N_1 + N_2 + N_3$.

3.2. The Deriving of Closed-Form Expression with Consecutive Elements. The 2-SC of the proposed array ranges from $2d$ to $2N_3(N_2 + 1)(N_1 + 1)d$, which is not a virtual consecutive array. It is worth noting that there are N_3 TL-NAs and a THL-NA with the same array structure in the 2-SC. In fact, the 2-SC can be regarded as the panning of a certain position of the proposed array. For instance, the THL-NA at the last part of the 2-SC can be regarded as the number of elements position in the physical array plus the largest number of elements position, which can be understood as the panning of the initial physical array.

Proposition 2. *The 2-SC can be divided into $N_3 + 1$ parts. The 2-SC position of THL-NA can be represented as*

Proposition 3. *The 2-DCSC position of THL-NA can be represented as*

$$S_{2\text{-DCSC}} = \{-2N_3(N_2 + 1)(N_1 + 1) + 2, \dots, -1, 0, 1, \dots, 2N_3(N_2 + 1)(N_1 + 1) - 2\}. \quad (29)$$

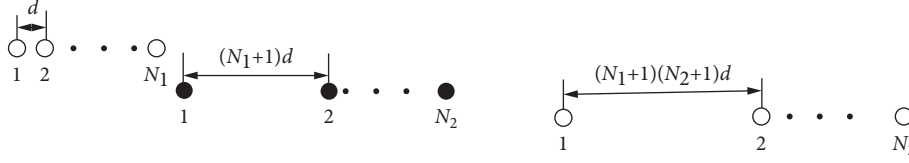


FIGURE 2: Three-level nested array structure.

Summarize the closed-form expression with the number of the consecutive lags of the array structure based on FOC as follows:

$$\begin{aligned} c\text{DOF} &= 2[2N_3(N_2 + 1)(N_1 + 1) - 2] + 1 \\ &= 4N_3(N_2 + 1)(N_1 + 1) - 3. \end{aligned} \quad (30)$$

Next, a specific array configuration example is used to deepen understanding. Figure 3 shows when the array configuration satisfies $N_1 = 3, N_2 = 3, N_3 = 4$, the position of physical sensors in the proposed array, the position of

array elements in the 2-SC and 2-DCSC. Next, the specific example is used to analyze and discuss the structure and properties of the proposed array.

The location of the physical sensors is distributed in $\{0.5, 1, 1.5, 2, 4, 6, 8, 16, 24, 32\}$. The 2-SC of the array ranges from $2d$ to $2N_3(N_2 + 1)(N_1 + 1)d$ namely 1 to 64 with $d = 0.5$. According to the above analysis, the 2-SC is divided into $N_3 + 1 = 5$ parts, and the position of coarray elements in each part can be expressed as

$$\begin{aligned} S_1 &= \{n_1 d, 2 \leq n_1 \leq (N_1 + 1)(N_2 + 1)\} \\ S_2 &= (N_1 + 1)(N_2 + 1)d + \{n_1 d, 1 \leq n_1 \leq N_1\} \cup \{n_2(N_1 + 1)d, 1 \leq n_2 \leq N_2 + 1\} \\ &= 8 + \{0.5, 1, 1.5, 2, 4, 6, 8\}, \\ S_3 &= 2(N_1 + 1)(N_2 + 1)d + \{n_1 d, 1 \leq n_1 \leq N_1\} \cup \{n_2(N_1 + 1)d, 1 \leq n_2 \leq N_2 + 1\} \\ &= 16 + \{0.5, 1, 1.5, 2, 4, 6, 8\}, \\ S_4 &= 3(N_1 + 1)(N_2 + 1)d + \{n_1 d, 1 \leq n_1 \leq N_1\} \cup \{n_2(N_1 + 1)d, 1 \leq n_2 \leq N_2 + 1\} \\ &= 24 + \{0.5, 1, 1.5, 2, 4, 6, 8\}, \\ S_5 &= 4(N_1 + 1)(N_2 + 1)d \\ &\quad + \{n_1 d, 1 \leq n_1 \leq N_1\} \cup \{n_2(N_1 + 1)d, 1 \leq n_2 \leq N_2\} \cup \{n_3(N_2 + 1)(N_1 + 1)d, 1 \leq n_3 \leq N_3\} \\ &= 32 + \{0.5, 1, 1.5, 2, 4, 6, 8, 16, 24, 32\}, \\ S_{2\text{-SC}} &= S_1 \cup S_2 \cup \dots \cup S_5. \end{aligned} \quad (31)$$

There is nested relationship among subarrays circled in the black box in Figure 3. The elements in the position set S_2, S_3, S_4 construct NA structure respectively, which can be regarded as TL-NA. The last part of the 2-SC is structurally equivalent to the proposed array, which can be regarded as a THL-NA. The consecutive 2-DCSC is obtained by performing a difference operation on the 2-SC. Since the 2-DC of the TL-NA is consecutive, the 2-DC of the sets S_2, S_3, S_4 is equivalent to the 2-DCSC of the proposed array, which is a consecutive virtual array. From Figure 3, it can be observed that the longest length of the consecutive holes is 8, and the longest length of the consecutive elements is 9. By performing the difference operation on set S_5 , a consecutive array is obtained. As a result, a consecutive virtual array can be obtained through the above array processing. The length of the consecutive DOF is $c\text{DOF} = 4N_3(N_2 + 1)(N_1 + 1) - 3 = 253$.

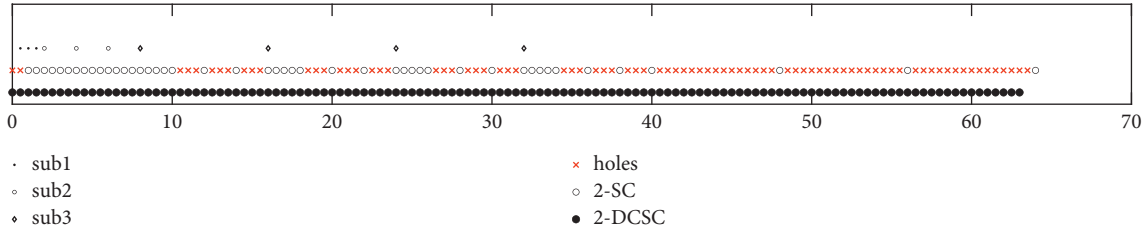
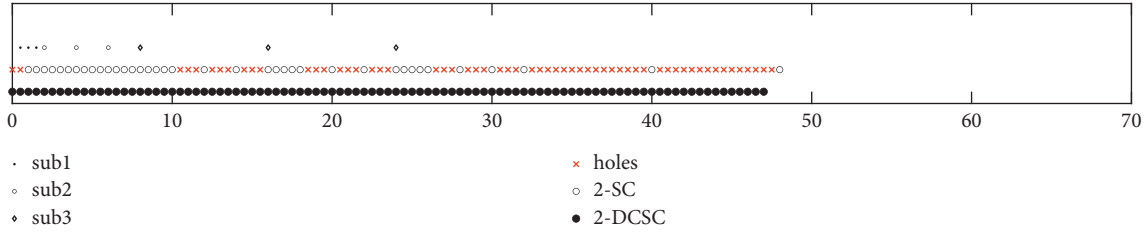
Figure 4 shows when the array configuration satisfies $N_1 = 3, N_2 = 3, N_3 = 3$, the position of physical sensors in the proposed array, the position of array elements in the 2-SC

and 2-DCSC. According to the above analysis, the consecutive DOF is $c\text{DOF} = 4N_3(N_2 + 1)(N_1 + 1) - 3 = 189$.

3.3. Optimal Array Configuration. For a fixed total number of physical sensors, there are multiple schemes about allocating sensors of each subarray in THL-NA. The problem of determining the optimal array configuration is addressed to maximize the consecutive DOF in this section. According to Proposition 3, the length of consecutive virtual elements in THL-NA is $4N_3(N_2 + 1)(N_1 + 1) - 3$. The consecutive DOF optimization problem can be formulated as

$$\begin{aligned} \max, & 4N_3N_2N_1 + 4N_3N_2 + 4N_3N_1 + 4N_3 - 3, \\ \text{subject to,} & N_3 + N_2 + N_1 = N. \end{aligned} \quad (32)$$

In equation (32), we focus on how to configure the number of sensors of each subarray (N_1, N_2, N_3) , so that the possible largest length of consecutive lags is obtained from


 FIGURE 3: The location of physical sensors, 2-SC, 2-DCSC when $N_1 = 3, N_2 = 3, N_3 = 4$.

 FIGURE 4: The location of physical sensors, 2-SC, 2-DCSC when $N_1 = 3, N_2 = 3, N_3 = 3$.

the virtual ULA when the total number of array sensors N is certain. We define integers m and n to be the remainder and quotient of N modulo 3, where $N = 3n + m$, $0 \leq m \leq 2$.

Proposition 4. *One solution to the optimization problem in equation (32) is can be presented as*

$$\begin{cases} N_3 = N_2 = N_1 = n, & \text{if } m = 0, \\ N_3 = n + 1, \quad N_2 = N_1 = n, & \text{if } m = 1, \\ N_3 = N_2 = n + 1, \quad N_1 = n, & \text{if } m = 2. \end{cases} \quad (33)$$

According to equation (33), the corresponding consecutive DOF can be evinced as

$$c - \text{DOF} = \begin{cases} 4n(n+1)(n+1) - 3, & \text{if } m = 0, \\ 4(n+1)(n+1)(n+1) - 3, & \text{if } m = 1, \\ 4(n+1)(n+2)(n+1) - 3, & \text{if } m = 2, \end{cases} \quad (34)$$

where $n = \lfloor N/3 \rfloor$.

Table 1 shows the consecutive degree of freedom corresponding to different array configurations when the number of physical sensors is 9. Proposition 4 can be verified with specific examples in Table 1.

4. The Proposed Algorithm

The computational complexity of the FOC matrix and that of the conventional MUSIC method due to the global spectrum

searching are expensive, the successive SS-MUSIC algorithm is presented, which employs partial spatial spectrum peak searching to drop the complexity. The SS-ESPRIT algorithm for the consecutive 2-DCSC of the THL-NA is utilized to obtain the initial estimates, which can be used to shrink the searching range of MUSIC algorithm to obtain the fine estimates.

4.1. Initial Estimates. From the previous discussion, there is a consecutive virtual array of the THL-NA with the range of elements $[-Wd, Wd]$, where $W = 2N_3(N_2 + 1)(N_1 + 1) - 2$, and the length of the virtual array is $T = 2W + 1$. Data model of the part refer to Section 2.3, the steering vector of the virtual array $\mathbf{a}^*(\theta_k) \in \mathbb{C}^{T \times 1}$ is denoted as

$$\mathbf{a}^*(\theta_k) = [e^{-j2\pi(-W)\sin\theta_k/\lambda}, \dots, 0, \dots, e^{-j2\pi W \sin\theta_k/\lambda}]^T. \quad (35)$$

According to the position of the virtual array, remove the redundant part of \mathbf{z} and sort \mathbf{z} , then construct \mathbf{z}_1 .

$$\mathbf{z}_1 = \Lambda_1 \mathbf{p}, \quad (36)$$

where $\Lambda_1 \in \mathbb{C}^{T \times K}$ is the direction matrix through sorting it after removing the redundant parts of $\Lambda(\theta)$, and its mathematical form can be represented by

$$\Lambda_1 = \begin{bmatrix} e^{-j(2\pi/\lambda)(-W)d \sin \theta_1} & e^{-j(2\pi/\lambda)(-W)d \sin \theta_2} & \dots & e^{-j(2\pi/\lambda)(-W)d \sin \theta_K} \\ \vdots & \vdots & \ddots & \vdots \\ 1 & 1 & 1 & 1 \\ \vdots & \vdots & \ddots & \vdots \\ e^{-j(2\pi/\lambda)Wd \sin \theta_1} & e^{-j(2\pi/\lambda)Wd \sin \theta_2} & \dots & e^{-j(2\pi/\lambda)Wd \sin \theta_K} \end{bmatrix}. \quad (37)$$

TABLE 1: C-DOF of different array configurations.

(N_1, N_2, N_3)	3, 3, 3	2, 3, 4	3, 2, 4	2, 4, 3	4, 2, 3	4, 3, 2	3, 4, 2	2, 2, 5	5, 2, 2	2, 5, 2
c-DOF	189	189	189	177	177	157	157	177	141	141

Under the situation, the traditional DOA algorithms, which use the eigenvalue decomposition of covariance, is invalid because of the vectorized interrelated signal. The received signal matrix is updated by intercepting the consecutive part of \mathbf{z}_1 . After obtaining the consecutive vector \mathbf{z}_1 , the spatial smoothing algorithm [19, 20], which divides the ULA into several overlapping subarrays, is exploited to take the place of the invalid traditional DOA algorithms. After obtaining the sum of the covariance matrices of the divided subarrays, which have the same array structure, the spatial smoothing covariance matrix is obtained by taking the average of it. As shown in Figure 5, $W + 1$ overlapping subarrays are obtained by dividing equally the virtual array, and each subarray incorporates $W + 1$ elements. Where, the sensors position of the i -th subarray is

$$\{(-i + 1 + n)d, n = 0, 1, \dots, W\}. \quad (38)$$

The received signal matrix \mathbf{z}_{1i} is from row $W + 2 - i$ to row $2W + 2 - i$ of \mathbf{z}_1 . Construct the covariance matrix:

$$\mathbf{R}_i = \mathbf{z}_{1i} \mathbf{z}_{1i}^H. \quad (39)$$

To obtain the spatial smoothing covariance matrix \mathbf{R} , which has the same form as the signal covariance matrix based on classical subspace algorithms, we sum the covariance matrices of all $W + 1$ subarrays and calculate the mean of it as shown in

$$\mathbf{R} = \frac{1}{W + 1} \sum_{i=1}^{W+1} \mathbf{R}_i. \quad (40)$$

In the following, the results of DOA estimation are obtained by using the classic ESPRIT algorithm [33]. Perform eigenvalue decomposition on \mathbf{R} to obtain the signal subspace \mathbf{U}_S and the noise subspace \mathbf{U}_N .

$$\mathbf{R} = \mathbf{U}_S \sum_S \mathbf{U}_S^H + \mathbf{U}_N \sum_N \mathbf{U}_N^H. \quad (41)$$

The rotation invariance of array makes the matrix \mathbf{U}_S decomposed into $\mathbf{U}_X \in \mathbb{C}^{(W-1) \times K}$, $\mathbf{U}_Y \in \mathbb{C}^{(W-1) \times K}$, corresponding to two subarrays, namely,

$$\mathbf{U}_S = \begin{bmatrix} \mathbf{U}_X \\ \mathbf{U}_Y \end{bmatrix} = \begin{bmatrix} \mathbf{U}_X \\ \mathbf{U}_X \mathbf{\Psi} \end{bmatrix}, \quad (42)$$

$$\mathbf{\Psi} = \mathbf{T}^{-1} \mathbf{\Phi} \mathbf{T}.$$

The signal subspace \mathbf{U}_X is similar to \mathbf{U}_Y , and the diagonal elements of $\mathbf{\Phi}$ are equal to the eigenvalues of $\mathbf{\Psi}$, so by calculating the eigenvalues λ_k of $\mathbf{\Psi} = \mathbf{U}_X^+ \mathbf{U}_Y$, where ($k = 1, 2, \dots, K$), the diagonal elements of $\mathbf{\Phi}$ is estimated to obtain the angle estimation value:

$$\hat{\theta}_k^{ini} = \arcsin\left(\text{angle} \frac{(\lambda_k)}{2\pi d}\right). \quad (43)$$

4.2. *Fine Estimates.* The initial estimated angles $\hat{\theta}_k^{ini}$ are employed to shrink the range of spectrum searching and the MUSIC algorithm is utilized to perform interval processing on the spatial spectrum function, where the interval range is expressed by $[\hat{\theta}_k^{ini} - \Delta, \hat{\theta}_k^{ini} + \Delta]$ (Δ is a small number), and then the more accurate angle estimation parameters are obtained.

The spatial spectrum function of MUSIC algorithm can be constructed as

$$P_{\text{MUSIC}} = \frac{1}{\mathbf{a}^H(\theta) \mathbf{U}_N \mathbf{U}_N^H \mathbf{a}(\theta)}, \quad (44)$$

where $\mathbf{a}(\theta)$ is the direction vector, and $\mathbf{a}(\theta) = [1, e^{-j2\pi \sin \theta/\lambda}, \dots, e^{-j2\pi(W-1)\sin \theta/\lambda}]^T \in \mathbb{C}^{W \times 1}$. While changing the value of θ , and performing the spectrum searching in the space domain. When the denominator of the spectral function tends to 0, in where the spatial spectral function reaches a peak, the noise vector is orthogonal to the signal vector, and the signal arrival angle $\hat{\theta}_k$ is equivalent as θ at this time.

4.3. *The Advantages of the Proposed Algorithm.* The main advantages of the proposed algorithm can be summarized as follows:

- (1) The computational complexity of the successive SS-MUSIC algorithm is much lower than SS-MUSIC algorithm
- (2) The successive SS-MUSIC algorithm owns approximately the same DOA estimation performance as the SS-MUSIC algorithm
- (3) The successive SS-MUSIC algorithm makes a balance between computational complexity and estimation accuracy

5. Performance Analysis

Aiming to evaluate the performance of the proposed array geometry and the proposed algorithm, the array performance index, including the consecutive DOF, the array aperture, the SS-MUSIC spectrum, the coupling leakage e.g., and the computational complexity are compared in this section.

5.1. *Analysis of the Proposed Array.* Direction of arrival In this part, we compare the consecutive DOF of ACA, SAFE-CPA, TL-NA, FL-NA, and THL-NA, as shown in Figure 6. Figure 6 demonstrates that the THL-NA has a higher consecutive DOF than other arrays. It is worth noting that when the number of array elements exceeds 12, the consecutive DOF of the THL-NA begins to be lower than that of FL-NA. From the overall trend of the image, the consecutive

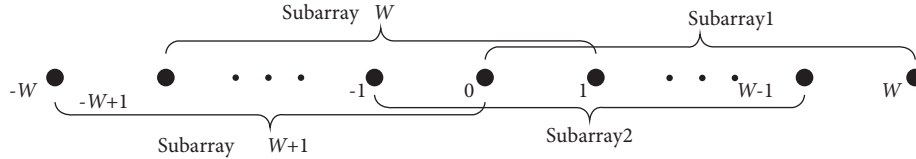


FIGURE 5: The spatial smoothing algorithm.

DOF of the THL-NA is close to but still greater than SAFE-CPA, which always surpasses that of FL-NA and TL-NA.

Table 2 lists the number of sensors, the consecutive DOF and the location of different arrays with 10 sensors. The length of array aperture in the proposed array is larger than that in TL-NA, ACA, which is smaller than that in FL-NA, SAFE-CPA.

$$M_0 = 4N_1N_2N_3 + 3N_1N_2 + 2N_1N_3 - N_2N_3 + N_1 - N_2 + N_3 - 1. \quad (45)$$

Table 3 shows the position, consecutive DOF, the weight distribution diagrams of the 2-SC, 2-DCSC, the SS-MUSIC spatial spectrum and mutual coupling coefficients of each array with 10 sensors in ACA, TL-NA, FL-NA, SAFE-CPA, THL-NA, and the consecutive DOF of the 2-DCSC with the THL-NA, SAFE-CPA, CPA, FL-NA, TL-NA can reach 253, 241, 85, 215, 117 respectively. The incident angles are evenly distributed between -50 and 50 , $\text{SNR} = 0\text{dB}$, SNAPSHOTS as $L = 500$.

The comparison of the MUSIC spatial spectrum of the array structure proposed in this paper with SAFE-CPA, CPA, FL-NA, TL-NA at the same incident angles is shown as Table 3. It can be seen that the incident angle information of all signals can be effectively detected only in the spectral peak diagram of the THL-NA, while the DOA estimation based on the other four arrays fail to find target estimation and search false peaks, which fully demonstrates that the THL-NA is capable of achieving higher accuracy DOA estimation.

5.2. Analysis of the Proposed Algorithm. For evaluating the proposed algorithm, the computational complexity is introduced into the analysis in this part, which is compared among the SS-MUSIC algorithm, the SS-ESPRIT method and the proposed algorithm. Specifically, the total number of sensors is N , the number of signal source is K , L indicates the number of snapshots, and the total number of the virtual array is $T = 2W + 1$, where $W = 2N_3(N_2 + 1)(N_1 + 1) - 2$.

Based on the number of complex multiplications, the main complexities of the methods involve that, the calculation of FOC matrix needs $O(LN^4)$. The virtual array is divided into $W + 1$ overlapping subarrays, and each subarray contains $W + 1$ elements. After the operation of spatial smoothing, the covariance matrix calculation of each virtual subarray needs $O\{(W + 1)^3\}$ and eigenvalue decomposition of the covariance matrix requires $O\{(W + 1)^3\}$, calculating Ψ needs $O\{2K^3 + 3K^2W\}$ and the eigenvalue decomposition

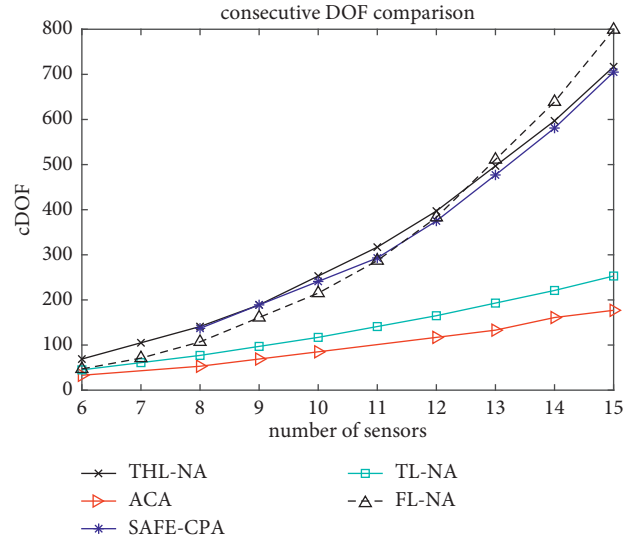


FIGURE 6: c-DOF comparison versus different arrays.

of Ψ requires $O\{K^3\}$. The complexity of spectral peak searching is $O\{n_1(W + 1)(2(W - K) + 3)\}$, where the number of searching $n_1 = 2K\Delta/0.01$, where Δ is a very small number and 0.01 is the searching accuracy.

Consequently, the total complexity of the proposed algorithm is given by $O\{LN^4 + 2(W + 1)^3 + 3K^2(W + K) + n_1(W + 1)(2(W - K) + 3)\}$, the total complexity of SS-ESPRIT algorithm is $O\{LN^4 + 2(W + 1)^3 + 3K^2(W + K)\}$, the total complexity of SS-MUSIC algorithm is $O\{LN^4 + 2(W + 1)^3 + n(W + 1)(2(W - K) + 3)\}$, where $n = 90/0.01$ stands for the peak search times over angle domain.

The computational complexity of algorithms is exhibited in Table 4. The histogram and the line graph are utilized to display the comparison results between the complexity of the three algorithms, as shown in Figures 7 and 8 respectively, where $K = 2$ and $L = 500$ in comparison versus different elements and $N_1 = 3, N_2 = 3, N_3 = 4$ in comparison versus different snapshots. It is observed that the complexity of the proposed algorithm is significantly lower than the SS-MUSIC method but is higher than the SS-ESPRIT algorithm.

6. RMSE Results

In this section, the root mean square error (RMSE) via 200 Monte-Carlo trials are utilized to validate the superior performance of the proposed array and the proposed algorithm by comparing with four arrays and two algorithms, respectively. The RMSE is defined by [34, 35]

TABLE 2: Comparison of the closed-form expression with consecutive DOF.

Arrays structure	Number of sensors ($N_i, i = 1, 2, \dots, 4$)	Consecutive DOF ($N_i, i = 1, 2, \dots, 4$)	Location ($T = 10$)
TL-NA	$N_1 + N_2$	$4N_2(N_1 + 1) - 3$	{0.5, 1, 1.5, 2, 2.5, 3, 6, 9, 12, 15}
FL-NA	$\sum_{i=1}^4 N_i - 3$	$2 \prod_{i=1}^4 N_i - 1$	{0.5, 1, 1.5, 2, 4, 6, 12, 18, 36, 54}
ACA	$2N_1 + N_2 - 1$	$6N_1N_2 + 2N_1 - 2N_2 - 1$	{0, 1.5, 2.5, 3, 4.5, 5, 6, 7.5, 10, 12.5}
SAFE-CPA	$2N_1 + N_2 - 1 + N_3$	$2M_0 + 1$	{0, 1, 1.5, 2, 3, 4.5, 17.5, 30.5, 43.5, 56.5}
Proposed	$N_1 + N_2 + N_3$	$4N_3(N_2 + 1)(N_1 + 1) - 3$	{0.5, 1, 1.5, 2, 4, 6, 8, 16, 24, 32}

TABLE 3: The 2-SC, 2-DCSC, c-DOF, spectrum, and $L(M)$ comparison of different arrays.

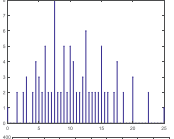
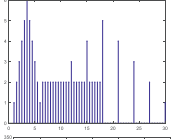
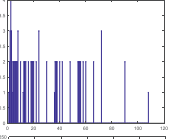
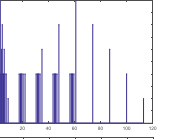
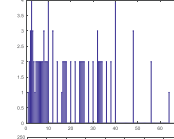
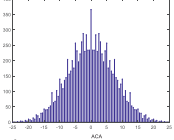
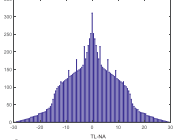
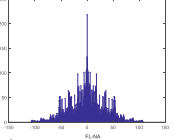
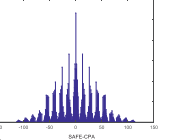
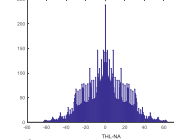
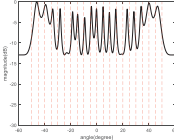
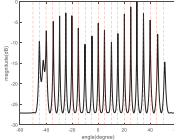
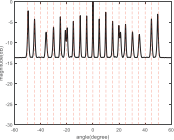
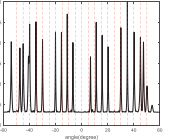
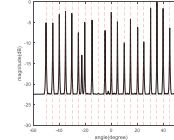
	ACA	TL-NA	FL-NA	SAFE-CPA	THL-NA
Antennas	{0, 1.5, 2.5, 3, 4.5, 5, 6, 7.5, 10, 12.5}	{0.5, 1, 1.5, 2, 2.5, 3, 6, 9, 12, 15}	{0.5, 1, 1.5, 2, 4, 6, 12, 18, 36, 54}	{0, 1, 1.5, 2, 3, 4.5, 17.5, 30.5, 43.5, 56.5}	{0.5, 1, 1.5, 2, 4, 6, 8, 16, 24, 32}
2-SC locations					
2-DCSC locations					
Spectrum					
C-DOF	85	117	215	241	253
$L(M)$	0.4582	0.6363	0.4686	0.4409	0.4728

TABLE 4: Complexity of different algorithms.

Algorithm	Computational complexity
Proposed	$O\{LN^4 + 2(W + 1)^3 + 3K^2(W + K) + n_1(W + 1)(2(W - K) + 3)\}$
SS-ESPRIT	$O\{LN^4 + 2(W + 1)^3 + 3K^2(W + K)\}$
SS-MUSIC	$O\{LN^4 + 2(W + 1)^3 + n(W + 1)(2(W - K) + 3)\}$

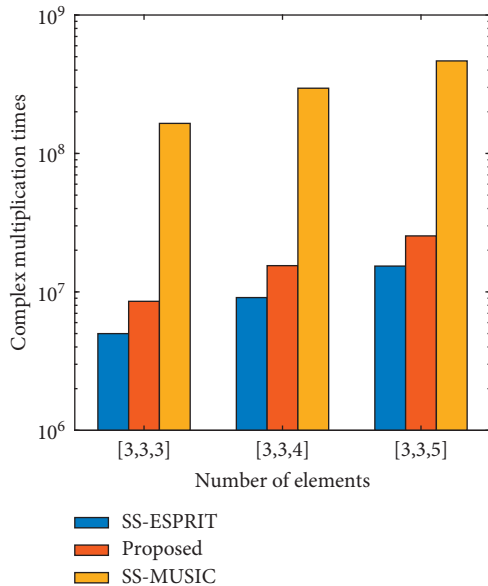


FIGURE 7: Complexities of different methods versus different elements.

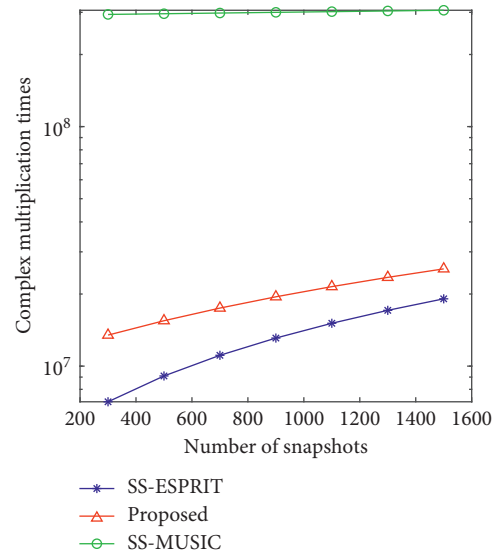


FIGURE 8: Complexities of different methods versus different snapshots.

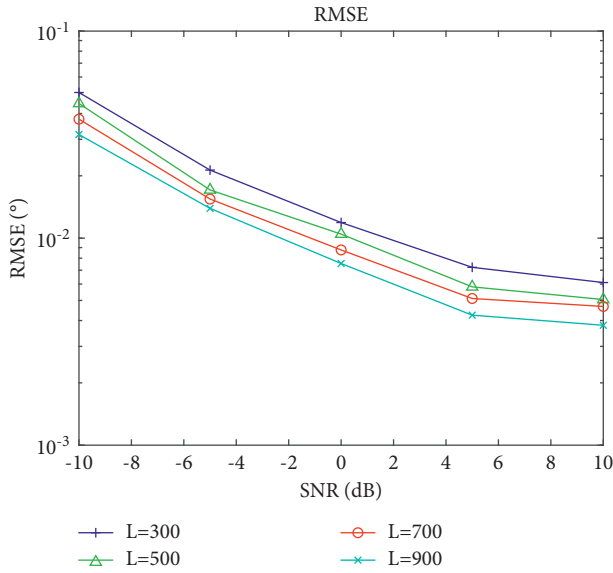


FIGURE 9: RMSE performance of different snapshots versus SNR.

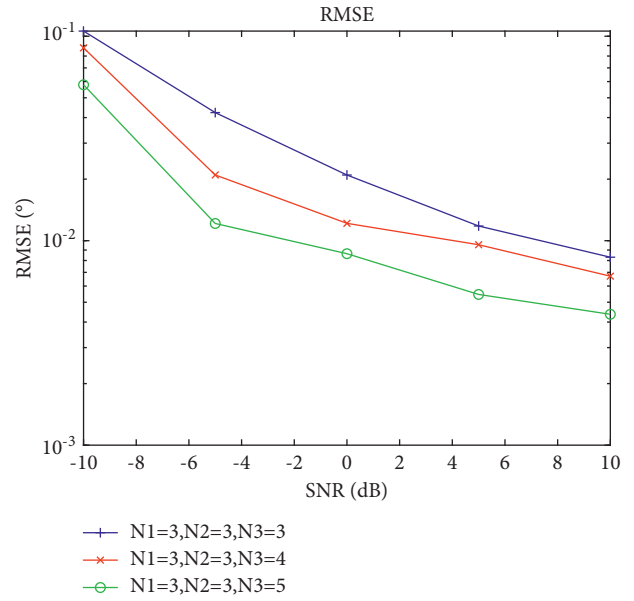


FIGURE 10: RMSE performance of different array configurations versus SNR.

$$\text{RMSE} = \frac{1}{K} \sum_{k=1}^K \sqrt{\frac{1}{200} \sum_{l=1}^{200} (\hat{\theta}_{k,l} - \theta_k)^2}, \quad (46)$$

where θ_k denotes the true elevation of the k -th target, $\hat{\theta}_{k,l}$ is estimated value of θ_k in the l -th ($l = 1, \dots, 200$) Monte-Carlo simulation. The non-Gaussian sources with $\theta = [5^\circ, 45^\circ]$ incident on the proposed array, SAFE-CPA, ACA, FL-NA, TL-NA, the total number of physical sensors is set as 10, and the consecutive DOF of the virtual coarray with the proposed array, SAFE-CPA, ACA, FL-NA, and TL-NA can reach 253, 241, 85, 215, and 117, respectively.

Sections 6.1–6.3 all employ the proposed successive SS-MUSIC algorithm to conduct the simulation experiments. Furthermore, Section 6.4 performs the comparison of different algorithms based on the proposed array geometry.

6.1. RMSE Comparison versus Snapshots. Figure 9 substantiates the effectiveness of the proposed array in estimated accuracy, and manifests that the increase of sampled data leads to the improvement of estimation performance, owing to the more accurate covariance estimation.

6.2. RMSE Comparison of Different Array Configurations. In this simulation, we compare the RMSE results of different array configurations, involving $N_1 = 3, N_2 = 3, N_3 = 3$, $N_1 = 3, N_2 = 3, N_3 = 4$ and $N_1 = 3, N_2 = 3, N_3 = 5$, using the successive SS-MUSIC algorithm, where SNAPSHOTS = 500. Meanwhile, the RMSE results of each algorithm versus the number of snapshots are exhibited in Figure 10. As depicted in Figure 10, with the number of elements increasing, the parameter estimation performance is enhanced because of diversity gain.

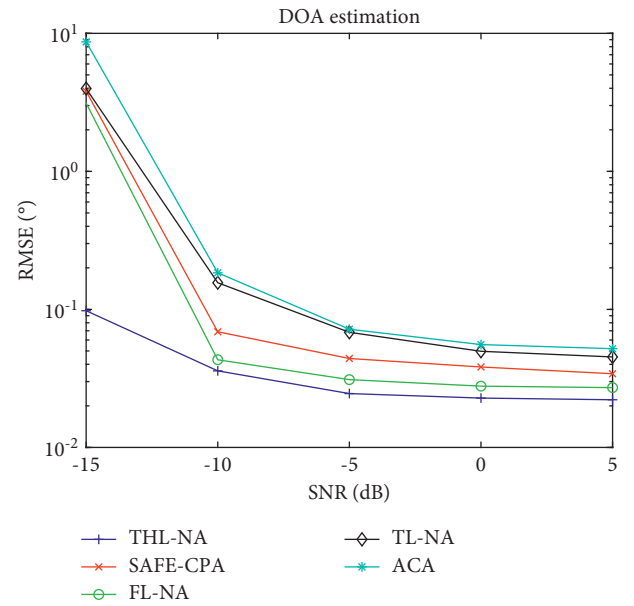


FIGURE 11: RMSE performance of different arrays versus SNR.

6.3. RMSE Performance Comparison of Different Arrays. To specifically examine the DOA estimation ability of the proposed array, the experiment uses 200 independent Monte Carlo experiments to statistically compares the RMSE of the array structure proposed in this paper with SAFE-CPA, ACA, FL-NA, TL-NA at different signal-to-noise ratios and snapshots, respectively. The number of physical sensors is 10. It is obviously seen that the performance of the proposed array is better than others.

Figure 11 presents the RMSE comparison of DOA estimation in different arrays versus SNR, where SNR is from -15 dB to 5 dB and SNAPSHOTS = 500. With the increase of

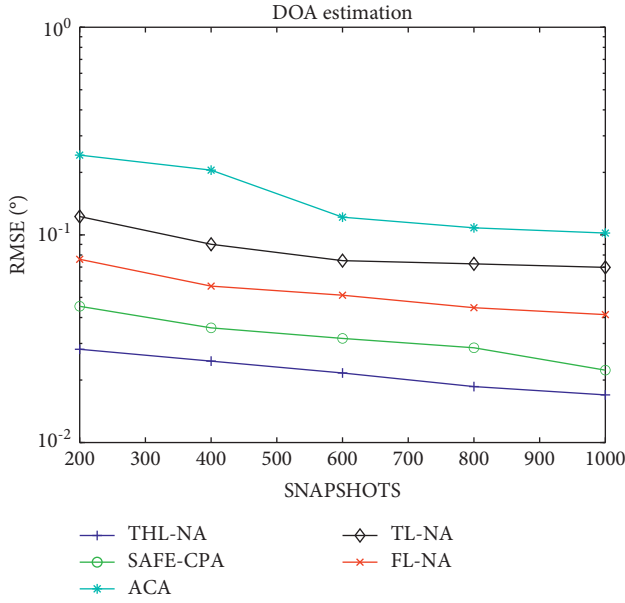


FIGURE 12: RMSE performance of different arrays versus SNAPSHOTS.

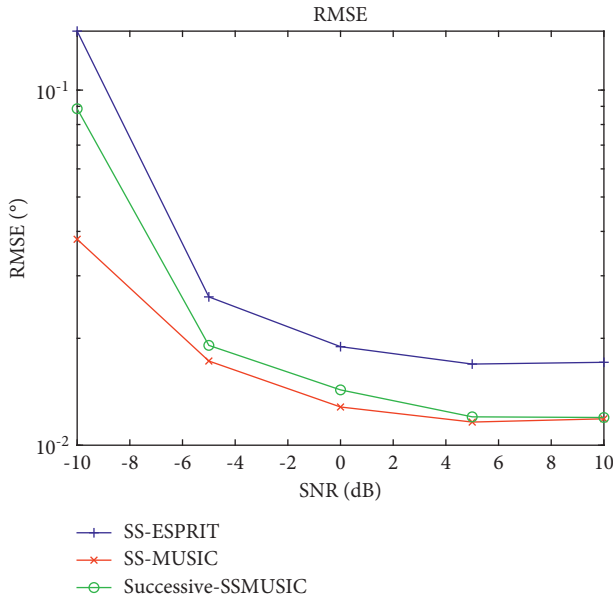


FIGURE 13: RMSE performance of different algorithms.

SNR, the THL-NA can reach the best DOA estimation performance compared to SAFE-CPA, ACA, FL-NA, and TL-NA.

Figure 12 presents the RMSE comparison of DOA estimation in different arrays versus SNAPSHOTS, where SNAPSHOTS is from 200 to 1000 and SNR = -5 dB. With the increase of the SNAPSHOTS, the THL-NA can reach the best DOA estimation performance compared to SAFE-CPA, ACA, FL-NA, and TL-NA due to the largest consecutive DOF.

6.4. RMSE Comparison of Different Algorithms. Figure 13 gives the comparison of estimation performance with

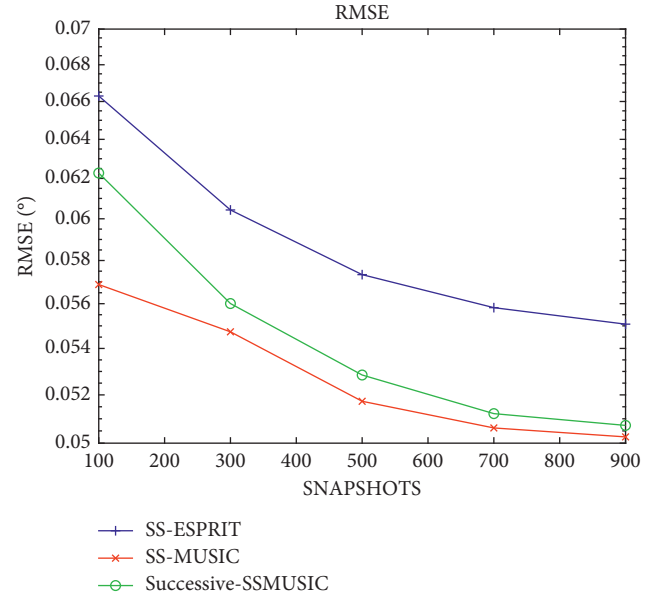


FIGURE 14: RMSE performance of different algorithms.

different algorithms versus SNR, where SNAPSHOTS = 500. In addition, the searching range of the successive SS-MUSIC algorithm and the SS-MUSIC method is $(\theta_k^{ini} - 1^\circ, \theta_k^{ini} + 1^\circ), k = 1, \dots, K$ and $(-60^\circ, 60^\circ)$, where θ_k^{ini} represents the initial DOA estimates according to Section 4.3. In terms of estimated performance according to following image, the successive SS-MUSIC algorithm is close to SS-MUSIC method and far better than SS-ESPRIT algorithm.

Figure 14 gives the comparison of estimation performance with different algorithms versus snapshots, where SNR = 0. It can be concluded from Figures 12 and 13 that the DOA estimation performance of the successive SS-MUSIC algorithm is more accurate than the SS-ESPRIT algorithm and slightly worse than the SS-MUSIC algorithm.

7. Conclusion

In this paper, the THL-NA is proposed for DOA estimation of non-Gaussian signals based on FOC, which can provide large consecutive DOF and a specific closed-form expression. The proposed array utilizes the characteristic of consecutive coarrays in TL-NA. Firstly, the array aperture is enlarged by obtaining the 2-SC of the proposed array, and then the nested relationship between subarrays in the 2-SC is employed to obtain 2-DCSC to construct a consecutive virtual array. The simulation results prove that the proposed array has higher performance than SAFE-CPA, CPA, FL-NA, TL-NA in DOA estimation. Besides, the successive SS-MUSIC method proposed in the paper has lower computational complexity than SS-MUSIC algorithm and more accurate estimate than SS-ESPRIT algorithm. In future research, sparse array design under the incidence of non-Gaussian sources based on MIMO system [36, 37] may be considered.

Data Availability

The data used to support the findings of this study are available from the corresponding author upon reasonable request.

Conflicts of Interest

The authors declare that they have no conflicts of interest.

Acknowledgments

This work was supported by China NSF (Grants 61971217, 61971218, and 61631020), Jiangsu NSF (Grant BK20200444), and National Key Research and Development Project (Grant 2020YFB1807602).

References

- [1] X. Zhang, L. Xu, L. Xu, and D. Xu, "Direction of departure (DOD) and direction of arrival (DOA) estimation in MIMO radar with reduced-dimension MUSIC," *IEEE Communications Letters*, vol. 14, no. 12, pp. 1161–1163, 2010.
- [2] J. Li, X. Zhang, and H. Chen, "Improved two-dimensional DOA estimation algorithm for two-parallel uniform linear arrays using propagator method," *Signal Processing*, vol. 92, no. 12, pp. 3032–3038, 2012.
- [3] F. Wen, "Computationally efficient DOA estimation algorithm for MIMO radar with imperfect waveforms," *IEEE Communications Letters*, vol. 23, no. 6, pp. 1037–1040, 2019.
- [4] P. Pal and P. P. Vaidyanathan, "Nested arrays: a novel approach to array processing with enhanced degrees of freedom," *IEEE Transactions on Signal Processing*, vol. 58, no. 8, pp. 4167–4181, 2010.
- [5] P. P. Vaidyanathan and P. Pal, "Sparse sensing with Co-prime samplers and arrays," *IEEE Transactions on Signal Processing*, vol. 59, no. 2, pp. 573–586, 2011.
- [6] P. P. Vaidyanathan and P. Pal, "Theory of sparse coprime sensing in multiple dimensions," *IEEE Transactions on Signal Processing*, vol. 59, no. 8, pp. 3592–3608, 2011.
- [7] R. Schmidt, "Multiple emitter location and signal parameter estimation," *IEEE Transactions on Antennas and Propagation*, vol. 34, no. 3, pp. 276–280, 1986.
- [8] M. Pesavento, A. B. Gershman, and M. Haardt, "Unitary root-MUSIC with a real-valued eigendecomposition: a theoretical and experimental performance study," *IEEE Transactions on Signal Processing*, vol. 48, no. 5, pp. 1306–1314, 2000.
- [9] R. Roy and T. Kailath, "ESPRIT-Estimation of signal parameters via rotational invariance techniques," *IEEE Transactions on Acoustics, Speech, & Signal Processing*, vol. 37, no. 7, pp. 984–995, 1986.
- [10] M. Haardt and J. A. Nosske, "Unitary ESPRIT: how to obtain increased estimation accuracy with a reduced computational burden," *IEEE Transactions on Signal Processing*, vol. 43, no. 5, pp. 1232–1242, 1995.
- [11] J. K. Tugnait, "On time delay estimation with unknown spatially correlated Gaussian noise using fourth-order cumulants and cross cumulants," *IEEE Transactions on Signal Processing*, vol. 39, no. 6, pp. 1258–1267, 1991.
- [12] M. C. Dogan and J. M. Mendel, "Applications of cumulants to array processing. II. Non-Gaussian noise suppression," *IEEE Transactions on Signal Processing*, vol. 43, no. 7, pp. 1663–1676, 1995.
- [13] B. Porat and B. Friedlander, "Direction finding algorithms based on high-order statistics," *IEEE Transactions on Signal Processing*, vol. 39, no. 9, pp. 2016–2024, 1991.
- [14] N. Yuen and B. Friedlander, "Asymptotic performance analysis of ESPRIT, higher order ESPRIT, and virtual ESPRIT algorithms," *IEEE Transactions on Signal Processing*, vol. 44, no. 10, pp. 2537–2550, 1996.
- [15] M. C. Dogan and J. M. Mendel, "Joint array calibration and direction-finding with virtual-ESPRIT algorithm," in *Proceedings of the IEEE Signal Processing Workshop on Higher-Order Statistics*, pp. 146–150, South Lake Tahoe, CA, USA, June 1993.
- [16] P. Pal and P. P. Vaidyanathan, "Multiple level nested array: an efficient geometry for $2q$ th order cumulant based array processing," *IEEE Transactions on Signal Processing*, vol. 60, no. 3, pp. 1253–1269, 2012.
- [17] E. BouDaher, F. Ahmad, and M. G. Amin, "Sparsity-based direction finding of coherent and uncorrelated targets using active nonuniform arrays," *IEEE Signal Processing Letters*, vol. 22, no. 10, pp. 1628–1632, 2015.
- [18] Q. Shen, W. Liu, W. Cui, and S. Wu, "Extension of Co-prime arrays based on the fourth-order difference Co-array concept," *IEEE Signal Processing Letters*, vol. 23, no. 5, pp. 615–619, 2016.
- [19] R. T. Williams, S. Prasad, A. K. Mahalanabis, and L. H. Sibul, "An improved spatial smoothing technique for bearing estimation in a multipath environment," *IEEE Transactions on Acoustics, Speech, & Signal Processing*, vol. 36, no. 4, pp. 425–432, 1988.
- [20] G.-T. Pham, P. Loubaton, and P. Vallet, "Performance analysis of spatial smoothing schemes in the context of large arrays," *IEEE Transactions on Signal Processing*, vol. 64, no. 1, pp. 160–172, 2016.
- [21] Z. Fu, P. Charge, and Y. Wang, "A virtual nested MIMO array exploiting fourth order difference coarray," *IEEE Signal Processing Letters*, vol. 27, pp. 1140–1144, 2020.
- [22] C. L. Liu and P. P. Vaidyanathan, "Super nested arrays: linear sparse arrays with reduced mutual coupling—part I: fundamentals," *IEEE Transactions on Signal Processing*, vol. 64, no. 15, pp. 3997–4012, 2016.
- [23] J. Liu, Y. Zhang, Y. Lu, S. Ren, and S. Cao, "Augmented nested arrays with enhanced DOF and reduced mutual coupling," *IEEE Transactions on Signal Processing*, vol. 65, no. 21, pp. 5549–5563, 2017.
- [24] Q. Shen, W. Liu, W. Cui, and S. Wu, "Extension of nested arrays with the fourth-order difference co-array enhancement," in *Proceedings of the 2016 IEEE International Conference on Acoustics, Speech and Signal Processing (ICASSP)*, pp. 2991–2995, Shanghai, China, March 2016.
- [25] X. Wang, L. T. Yang, D. Meng, M. Dong, K. Ota, and H. Wang, "Multi-UAV cooperative localization for marine targets based on weighted subspace fitting in SAGIN environment," *IEEE Internet of Things Journal*, 2021.
- [26] C. Ye, W. Chen, B. Zhu, and L. Tang, "Direction of arrival estimation of non-Gaussian signals for nested arrays: applying fourth-order difference co-array and the successive method," *ETRI Journal*, vol. 43, 2021.
- [27] Y. Zhang, D. Wang, H. Xu, S. Yang, Z. Wang, and J. You, "High-accuracy DOA estimation based on vectorized fourth-order cumulant with coprime array," in *Proceedings of the 2019 IEEE 19th International Conference on Communication Technology (ICCT)*, pp. 210–215, Xi'an, China, October 2019.
- [28] C. Liu and P. P. Vaidyanathan, "Super nested arrays: sparse arrays with less mutual coupling than nested arrays," in

- Proceedings of the 2016 IEEE International Conference on Acoustics, Speech and Signal Processing (ICASSP)*, pp. 2976–2980, Shanghai, China, March 2016.
- [29] J. Shi, G. Hu, X. Zhang, and H. Zhou, “Generalized nested array: optimization for degrees of freedom and mutual coupling,” *IEEE Communications Letters*, vol. 22, no. 6, pp. 1208–1211, 2018.
- [30] B. Liao, Z. G. Zhang, and S. C. Chan, “DOA estimation and tracking of ULAs with mutual coupling,” *IEEE Transactions on Aerospace and Electronic Systems*, vol. 48, no. 1, pp. 891–905, 2012.
- [31] B. Friedlander and A. J. Weiss, “Direction finding in the presence of mutual coupling,” *IEEE Transactions on Antennas and Propagation*, vol. 39, no. 3, pp. 273–284, 1991.
- [32] Z. Ye, J. Dai, X. Xu, and X. Wu, “DOA estimation for uniform linear array with mutual coupling,” *IEEE Transactions on Aerospace and Electronic Systems*, vol. 45, no. 1, pp. 280–288, 2009.
- [33] C. Wu and C. Ye, “DOA estimation for unfolded coprime arrays: successive-MUSIC algorithm,” *IOP Conference Series: Materials Science and Engineering*, vol. 719, 2020.
- [34] H. Wang, L. Wan, M. Dong, K. Ota, and X. Wang, “Assistant vehicle localization based on three collaborative base stations via SBL-based robust DOA estimation,” *IEEE Internet of Things Journal*, vol. 6, no. 3, pp. 5766–5777, 2019.
- [35] J. Cong, X. Wang, C. Yan, L. T. Yang, M. Dong, and K. Ota, “CRB weighted source localization method based on deep neural networks in multi-UAV network,” *IEEE Internet of Things Journal*, 2022.
- [36] G. Zheng, Y. Song, and C. Chen, “Height measurement with meter wave polarimetric MIMO radar: signal model and MUSIC-like algorithm,” *Signal Processing*, vol. 190, Article ID 108344, 2022.
- [37] G. Zheng and Y. Song, “Signal model and method for joint angle and range estimation of low-elevation target in meter-wave FDA-MIMO radar,” *IEEE Communications Letters*, vol. 26, no. 2, pp. 449–453, 2022.